Monthly Notices
of the
ROYAL ASTRONOMICAL SOCIETY

MNRAS **502,** 1569–1578 (2021)
Advance Access publication 2021 January 14

doi:10.1093/mnras/stab090

Modelling the delivery of dust from discs to ionized winds

Richard A. Booth [1]★ and Cathie J. Clarke[2]

[1]*Astrophysics Group, Imperial College London, Prince Consort Road, London SW7 2AZ, UK*
[2]*Institute of Astronomy, Madingley Road, Cambridge CB3 0HA, UK*

Accepted 2021 January 11. Received 2021 January 11; in original form 2020 December 10

ABSTRACT

A necessary first step for dust removal in protoplanetary disc winds is the delivery of dust from the disc to the wind. In the case of ionized winds, the disc and wind are sharply delineated by a narrow ionization front where the gas density and temperature vary by more than an order of magnitude. Using a novel method that is able to model the transport of dust across the ionization front in the presence of disc turbulence, we revisit the problem of dust delivery. Our results show that the delivery of dust to the wind is determined by the vertical gas flow through the disc induced by the mass-loss, rather than turbulent diffusion (unless the turbulence is strong, i.e. $\alpha \gtrsim 0.01$). Using these results, we provide a simple relation between the maximum size of particle that can be delivered to the wind and the local mass-loss rate per unit area from the wind. This relation is independent of the physical origin of the wind and predicts typical sizes in the 0.01–1 μm range for extreme-ultraviolet- or X-ray-driven winds. These values are a factor of ∼10 smaller than those obtained when considering only whether the wind is able to carry away the grains.

Key words: planetary systems – protoplanetary discs – stars: pre-main sequence – (ISM:) dust, extinction.

1 INTRODUCTION

Mass-loss in protoplanetary disc through winds is important for understanding their evolution. In particular, photoevaporative winds driven by X-rays, extreme-ultraviolet (EUV), or far-ultraviolet radiation are thought to be responsible for the final rapid clearing of protoplanetary discs (e.g. Clarke, Gendrin & Sotomayor 2001; Owen, Ercolano & Clarke 2011b; Ercolano et al. 2015; Gorti et al. 2016). More recently, magnetohydrodynamic (MHD) winds have replaced turbulence as being the most promising processes responsible for driving accretion in protoplanetary discs (Salmeron, Königl & Wardle 2007; Suzuki & Inutsuka 2009; Bai 2017; Béthune, Lesur & Ferreira 2017). As a result, the entrainment of dust in these winds has also become an important issue. Throop & Bally (2005) suggested that the preferential removal of gas by winds might aid planet formation, although more recent studies (Ercolano et al. 2017; Sellek, Booth & Clarke 2020) suggest that this is unlikely unless radial drift of dust can be suppressed. In addition, the dust entrained in winds may provide a way to probe them observationally (e.g. Owen, Ercolano & Clarke 2011a; Miotello et al. 2012; Franz et al. 2020).

The problem of dust entrainment may be thought of in two parts. First, there is the question of whether dust particles entering the wind region are sufficiently well coupled to the gas so as to be carried away by the wind. However, more importantly, such escaping dust grains also need to be *delivered* to the wind from the underlying disc. In the case of winds driven by EUV radiation, the wind and disc are sharply delineated by a narrow ionization front where the gas density and temperature vary by many orders of magnitude. Previously, Hutchison, Laibe & Maddison (2016) and Hutchison & Clarke (2021) have found that delivery is the limiting step in controlling the range of dust sizes that are lost in such winds.

In some previous studies (e.g. Hutchison et al. 2016), it has been assumed that dust delivery to the wind occurs diffusively, with turbulence in the disc competing against settling due to gravity to loft the grains into the wind. However, it has recently become clear that dust may instead be delivered to the wind *advectively*, through coupling of the motion of dust grains to the upward motion of gas towards the ionization front. Although this gas motion is strongly subsonic (likely even below the typical turbulent speeds), Hutchison & Clarke (2021) argued that advection is an important component in the delivery of dust to the wind. There is precedence for this, since in their MHD simulations of disc winds Riols & Lesur (2018) showed that advection resulted in an increase of the dust scale height over the height expected from purely turbulent transport.

However, Hutchison & Clarke (2021) encountered a problem in quantifying how efficiently dust is delivered to the wind. This problem was associated with the non-convergence of their results as the width of the ionization front was reduced. This non-convergence, as discussed in Hutchison & Clarke (2021), results from the fact that there is a steep gradient in gas density at the ionization front, where the gas goes from being cold in the disc to hot in the ionized wind. Although the gas velocity changes rapidly across the ionization front, changes in the dust velocity occur on a 'stopping time', t_s, the time over which drag forces act. This means that the dust density varies over the 'stopping length', vt_s. Since the stopping length can be much larger than the ionization front width, this leads to a steep increase of the dust-to-gas ratio across the ionization front. Hutchison & Clarke (2021) modelled the effects of turbulence as a diffusion equation (following Dubrulle, Morfill & Sterzik 1995) so that this large gradient in dust-to-gas ratio produced a large negative

★ E-mail: r.booth@imperial.ac.uk

diffusive flux. This flux then suppresses the delivery of dust to the wind, by an amount that depends on the width of the ionization front.

However, this approach is not fully consistent because the diffusion is ultimately driven by the coupling of the dust dynamics to turbulent gas motions via drag forces. Diffusive motions are therefore subject to the same constraints as the mean flow in being limited by the finite coupling between dust and gas. A reduction of the effective diffusion coefficient, in cases where the gas flow changes on scales less than the stopping distance, is, however, not captured by the formulation of Dubrulle et al. (1995), which therefore gives erroneous results in this limit.

The goal of this paper is to rectify this deficiency in modelling dust transport across narrow fronts, thus determining how efficiently dust is delivered to the wind. Instead of solving an advection–diffusion equation, we use a Monte Carlo model to trace the dynamics of individual dust grains, explicitly treating the coupling of the dust to turbulent velocity fluctuations in the disc gas. This approach is similar to the one used by Youdin & Lithwick (2007) to model the diffusion of large dust particles in discs, for example. We present our model in Section 2, and in Section 3 demonstrate that, in contrast to other formulations for modelling dust in turbulent flows in the literature, we are able to correctly recover the structure of the gas and dust across steep transitions in the gas density, an important prerequisite for tackling problems involving ionization fronts. In Section 4, we consider the two criteria suggested by Hutchison & Clarke (2021) as limiting the maximum size of grains that are (a) deliverable to the ionization front and (b) entrainable by the wind above the ionization front, for which the corresponding Stokes numbers (evaluated just below the ionization front) are denoted by $St_{\rm crit}$ and $St_{\rm max}$, respectively. We then use these limits to estimate the level of turbulence at which a transition between diffusive and advective feeding of dust into the wind base is expected. In Section 5, we demonstrate that, as anticipated by Hutchison & Clarke (2021), $St_{\rm crit}$ (which turns out to be ∼0.01 for a wide range of input parameters) indeed represents a good limit for setting the maximum size of dust delivered into the wind: Although somewhat larger dust grains may enter the wind in the limit of strong turbulence, the grains entering the wind have Stokes number significantly less than $St_{\rm max}$ and hence are all capable of being fully entrained in the ionized flow. A discussion of our results and conclusions are presented in Sections 6 and 7.

2 MODEL

2.1 Modelling the disc/wind base: gas

We model the entrainment of dust in a background disc undergoing photoevaporation. The vertical structure of the disc is computed by solving the momentum equation of hydrodynamics in one dimension:

$$u_z \frac{\partial u_z}{\partial z} = -\frac{1}{\rho}\frac{\partial \left[\rho c_{\rm s}(z)^2\right]}{\partial z} - \frac{GMz}{(R^2+z^2)^{3/2}}, \tag{1}$$

assuming a steady state such that ρu_z is constant. Here, u_z is the gas velocity and ρ is the gas density.

The sound-speed profile, $c_{\rm s}(z)$, is chosen to model the transition from a cold disc to a hot photoionized wind at the ionization front:

$$c_{\rm s}(z) = \frac{c_{\rm s,disc}+c_{\rm s,wind}}{2} + \frac{c_{\rm s,wind}-c_{\rm s,disc}}{2}\tanh\left(\frac{|z-z_{\rm IF}|}{3W}\right). \tag{2}$$

Here, disc is assumed to be vertically isothermal, where $c_{\rm s,disc}$ and $c_{\rm s,wind}$ denote the sound speed in the disc and wind, respectively, with $z_{\rm IF}$ and W specifying the location and width of the transition, respectively.

By default, we take $M = 1\,{\rm M}_\odot$ and $R = 10\,{\rm au}$. We assume that the disc aspect ratio is given by $H/R = 0.05(R/{\rm au})^{0.25}$; thus, $c_{\rm s,mid} \approx 0.84\,{\rm km\,s^{-1}}$. The sound speed in the wind is $c_{\rm s,wind} = 12.85\,{\rm km\,s^{-1}}$, appropriate for a fully ionized hydrogen gas at 10^4 K. Where required, the mid-plane density is taken to be $\rho_0 = \Sigma(R)/\sqrt{(2\pi)}H$, assuming the gas surface density $\Sigma(R) = 30(R/{\rm au})^{-1}\,{\rm g\,cm^{-3}}$.

To set the mid-plane velocity, we assume that photoionization drives an outflow with a velocity of $v_{\rm wind} = 0.5c_{\rm s,wind}$ at the ionization front; this being motivated by typical launch velocities for self-similar solutions for isothermal winds (Clarke & Alexander 2016). Explicitly, we find the velocity at $z = 0$ iteratively by integrating equation (1) to $z = z_{\rm IF} + 9W$ and requiring that v_z at this point is $0.5c_{\rm s,wind}$. The parameter $z_{\rm IF}$ controls the density at the base of the ionized wind $\rho_{\rm ion}$, once the mid-plane density and temperature of the disc are assigned. Since the disc below the ionization front is very close to a state of hydrostatic equilibrium, $\rho_{\rm ion} \sim \rho_0 \exp(-z_{\rm IF}^2/2H^2) f_i$, where f_i is the factor by which the density drops across the ionization front: $f_i \sim c_{\rm s,mid}^2/(c_{\rm s,wind}^2 + v_{\rm wind}^2)$. The canonical parameters detailed above and $\rho_{\rm ion}$ derived from equation (23) for an ionizing flux of $10^{42}\,{\rm s^{-1}}$ correspond to $z_{\rm IF} \sim 4H$. Assuming the standard profiles for photoevaporative winds driven by EUV radiation (Hollenbach et al. 1994), these values would correspond to integrated mass-loss rates from the disc of the order of (10^{-10})–$(10^{-9})\,{\rm M_\odot\,yr^{-1}}$.

Equation (1) is solved numerically using the fourth-order Runge–Kutta method of Dormand & Prince (e.g. Press et al. 2007) as implemented in the ODEINT package in the BOOST library.[1] The solution at intermediate points is then obtained via piecewise-cubic Hermite interpolation (Fritsch & Carlson 1980).

2.2 Modelling the disc/wind base: dust

The dust component is treated using a Stochastic Lagrangian model. We compute the trajectory of a large number of tracer particles under the action of gravity, coupled to the gas via drag forces:

$$\frac{{\rm d}z}{{\rm d}t} = v_z, \tag{3}$$

$$\frac{{\rm d}v_z}{{\rm d}t} = -\frac{v_z - [u_z(z) + u_z'(z,t)]}{t_{\rm stop}} - \frac{GMz}{(R^2+z^2)^{3/2}}, \tag{4}$$

where v_z is the vertical velocity of the dust. Here, we have decomposed the gas velocity into its background component and a fluctuating part, $u_z'(z,t)$, which represents the motions due to turbulence in the disc that are responsible for diffusion. We will assume that the turbulent fluctuations are Gaussian in nature with a correlation time, $t_{\rm e}$. We assume linear Epstein drag such that

$$t_{\rm stop} = \sqrt{\frac{\pi}{8}}\frac{\rho_{\rm grain} s}{c_{\rm s}\rho}, \tag{5}$$

where $\rho_{\rm grain}$ is the internal density of a dust grain and s is its size. Typically, we label grain size by their Stokes number, $St = t_{\rm s}\Omega$, but where relevant we will assume $\rho_{\rm grain} = 1\,{\rm g\,cm^{-3}}$. The background gas velocity, $u_z(z)$, sound speed, $c_{\rm s}$, and density, ρ, are taken from the model described in Section 2.1.

The turbulent fluctuations are treated using a Langevin model based on Thomson (1984) (see also Wilson, Legg & Thomson 1983). Thomson (1984) derived a Stochastic Lagrangian model for the motion of tracer particles in the atmosphere by requiring that the statistical distribution of the particles must be the same as that

[1] https://www.boost.org/

of the underlying atmosphere. Thomson (1987) showed that this requirement – that the particles must remain 'well mixed' with the gas – is rather general, with Stochastic Lagrangian models that satisfy this criterion being consistent with the Euler equations and able to reproduce both the short- and long-term behaviour of the gas. Under the assumption of Gaussian velocity fluctuations, the model for the gas is

$$\delta z = [u_z(z) + \sigma(z) w_t]\delta t, \tag{6}$$

$$\delta w_t = -\frac{(w_t - w_{hs})}{t_e}\delta t + \sqrt{\frac{2}{t_e}}\delta W, \tag{7}$$

where

$$w_{hs} = \sigma(z)\left\{\frac{1}{2}\frac{\partial \ln[\sigma(z)^2]}{\partial z} + \frac{\partial \ln[\rho(z)]}{\partial z}\right\} t_e. \tag{8}$$

The w_{hs} term corrects for the fact that that a Gaussian distribution of turbulent velocities with mean zero will drive a non-zero net flux when there are gradients in $\rho(z)$ or $\sigma(z)$ (Thomson 1984; Ciesla 2010). Here, t_e is the Lagrangian correlation time, $\sigma(z, t)^2$ is the variance of the velocity fluctuations, and W is Wiener Process; i.e. δW is a random number distributed as $\delta W \sim \mathcal{N}(0, \delta t)$ [where $\mathcal{N}(0, \delta t)$ is a normal distribution with mean zero and variance δt]. The diffusion coefficient D is linked to t_e and σ via $D = \sigma^2 t_e$ (e.g. Youdin & Lithwick 2007; Ormel & Liu 2018). By default, we take $t_e = \Omega^{-1}$, where Ω is the Keplerian frequency and $D = \alpha c_{s,disc}^2 \Omega^{-1}$, giving $\sigma = \sqrt{\alpha} c_{s,disc}$ so that the dimensionless parameter α relates the sound speed to the turbulent velocity as in the viscous α parametrization of Shakura & Sunyaev (1973).

We extend this model to treat dust grains in the simplest way possible, which is to use take $u_z'(z) = \sigma(z, t) w_t$ and use the particle's position to define z in equation (7). Explicitly, we use

$$\delta z = v_z \delta t, \tag{9}$$

$$\delta v_z = -\frac{v_z - [u_z(z) + \sigma(z) w_t]}{t_{stop}}\delta t - \frac{GMz}{(R^2 + z^2)^{3/2}}\delta t, \tag{10}$$

$$\delta w_t = -\frac{(w_t - w_{hs})}{t_e}\delta t + \sqrt{\frac{2}{t_e}}\delta W, \tag{11}$$

which reduces to Thomson (1984)'s model in the limit $t_{stop} \to 0$.

Our model is similar to, but differs from, existing Stochastic Lagrangian models for dust in the literature. For $u_z = 0$ and constant ρ, our model reduces to that of Youdin & Lithwick (2007). The model of Ormel & Liu (2018) is the most similar to ours, differing by the way in which the correction term w_{hs} is implemented. Ormel & Liu (2018) add a term σw_{hs} to u_z in equation (10) while neglecting w_{hs} in equation (11). When w_{hs} is slowly varying, the effect of this on the dynamics is small; however, in the presence of a sharp transition in the density (or turbulence), as is the case at an ionization front, the difference becomes significant. Since we apply the correction in equation (11), the effects of steep transition in density are averaged over t_e, whereas in the case of Ormel & Liu (2018) they are applied locally. The model proposed by Laibe, Bréhier & Lombart (2020) is equivalent to assuming $w_{hs} = 0$ in equation (11). These differences are highlighted in Section 3.[2]

[2]Ciesla (2010) also provided a Stochastic Lagrangian model that satisfies Thomson (1987)'s well-mixed condition. However, Ciesla (2010) used the terminal velocity approximation for the mean flow and, by imposing fixed (i.e. t_{stop} independent) velocity impulses, neglected the finite Lagrangian correlation time of the turbulence, making it inappropriate for the ionization front problem. Thus, we do not consider it further.

2.3 Implementation

We have adopted a semi-implicit approach to solve equations (9)–(11) efficiently for particles with short stopping times. First, we move the particle from z to $z + v_z \delta t$. Next, we update w_t, evaluating the right-hand side of equation (11) at the new position. Finally, we update the dust velocity, v_z, using the new position and w_t. This update is done implicitly in v_z to avoid limits on the time-step due to small t_{stop}, such that

$$v_z(t + \delta t) = \left[v_z(t) - \frac{GMz\delta t}{(R^2 + z^2)^{3/2}}\right]\frac{t_{stop}}{\delta t + t_{stop}} + [u_z(z) + \sigma(z) w_t]\frac{\delta t}{\delta t + t_{stop}}. \tag{12}$$

It is straightforward to verify that this expression is correct in the limits $t_{stop} \to 0$ and $t_{stop} \to \infty$.

The time-step, δt, is chosen to satisfy a number of constraints:

$$\begin{aligned}
\delta t_{max} &= \left[\delta t_0^{-1} + \delta t_1^{-1} + \delta t_2^{-1} + \delta t_3^{-1}\right]^{-1} \\
\delta t_0 &= 0.01 t_e \\
\delta t_1 &= 0.01\left(\frac{\partial \sigma}{\partial z}\right)^{-1} \\
\delta t_2 &= 0.01\left(\sigma\frac{\partial \ln \rho}{\partial z}\right)^{-1} \\
\delta t_3 &= 0.05\frac{\max(|z - z_{IF}|, W)}{v_z}.
\end{aligned}$$

The first three constraints are designed to ensure that w_t and w_{hs} do not change significantly in one time-step, while the last one is included to make sure that the particles do not jump across the ionization front in a single time-step.

Rather than setting $\delta t = \delta t_{max}$, we instead set $\delta t = 2^{\ell - \ell_{max}}\Omega^{-1}$, where $\ell_{max} = 63$ and ℓ is the largest integer such that $\delta t \leq \delta t_{max}$. Particle time-steps are always allowed to decrease; however, increases are only allowed if the particle would remain synchronized (i.e. t is exactly divisible by δt). This decision is made to ensure that all particles are synchronized every t_e, so that their positions and velocities can be sampled at the same time.

3 TESTS

To test the code, we compute the distribution of particles in a Gaussian disc with a constant sound speed and $u_z = 0$, comparing the results to the methods proposed by Ormel & Liu (2018) and Laibe et al. (2020). For each test, 10^3 particles were injected at $z = 0$. After a burn-in period of $10^4\Omega^{-1}$, the positions of each particle in the range $[-5, 5]$ (for $St = 0$ and $[-2, 2]$ for $St = 0.05$) were recorded every $10\Omega^{-1}$ for the next $10^5\Omega^{-1}$. The density was computed by binning the particles into 100 bins, normalized such that the total mass is 1.

First, we consider particles with $St = 0$, which should be distributed with the same density as the gas. Fig. 1 (left-hand panel) shows this for the case of a constant $\alpha = 0.01$. Here, both our method and Ormel & Liu (2018)[3] produce similar results, with the particles well mixed with the gas. However, the method of Laibe et al. (2020)

[3]Note that we updated the dust velocity implicitly, as in our method, rather than using Ormel & Liu (2018)'s 'Strong Coupling Approximation' since that method is not appropriate for our problem.

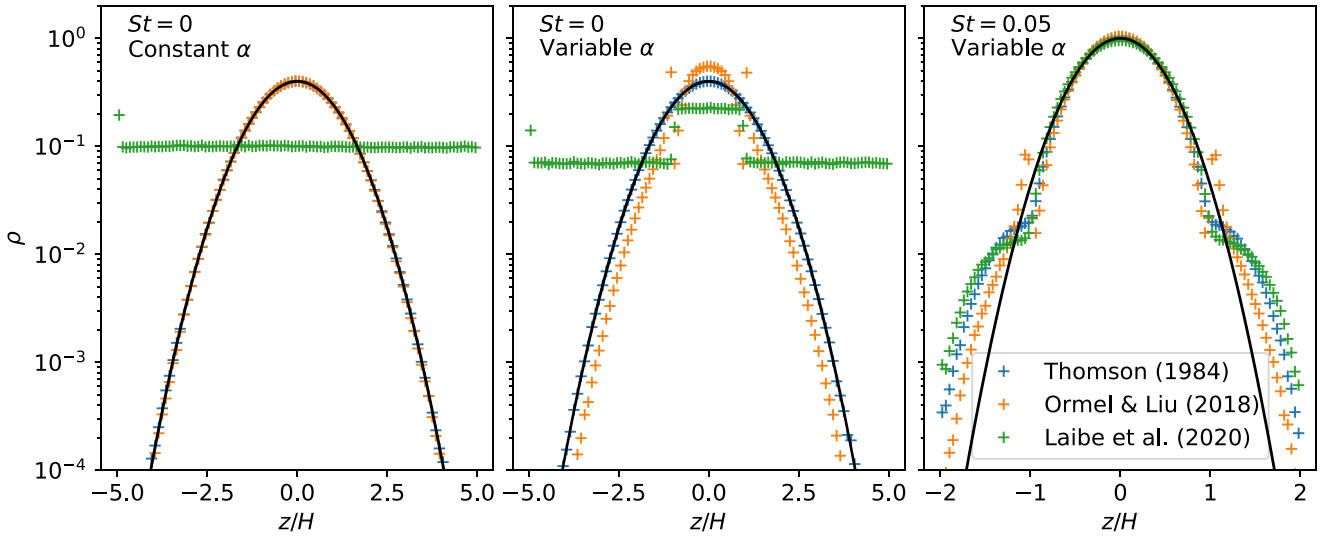

Figure 1. The vertical structure of gas and dust particles in a Gaussian disc computed with different Stochastic Lagrangian models. Left: A constant turbulent $\alpha = 0.01$ is used. Middle and right: α transitions from 0.01 to 0.1 at $z = H$. In each case, the black line shows the analytical solution (only valid close to the mid-plane for $St = 0.05$). Only the Thomson (1984) model (which we use in this paper) recovers a constant dust-to-gas ratio for $St = 0$ in the presence of steep gradients.

produces a constant dust density rather than dust-to-gas ratio, which is a consequence of neglecting the $w_{\rm hs}$ term.

Next, we consider the same model but with α varying from 0.01 to 0.1, using the functional form of equation (2) with $z_{\rm IF} = H$ and $W = H/60$. Note that $c_{\rm s}$ is constant in this test. Under these conditions, particles with $St = 0$ should still have the same density distribution as the gas. Now we see a difference between the method of Ormel & Liu (2018) and the one presented in this work, with only our method producing a constant dust-to-gas ratio. The 'blip' in the density around $z = H$ produced by Ormel & Liu (2018)'s method arises because $w_{\rm hs}$ is large at this location. When applied in equation (10), as in Ormel & Liu (2018), this leads to large velocities for the dust particles, which are responsible for the 'blip'. In our method, these large velocities are not produced because $w_{\rm hs}$ gets averaged over $t_{\rm e}$. We note that these differences are only significant if $w_{\rm hs}$ varies over a small length-scale – this was not the case in the tests presented in Ormel & Liu (2018), but such variations do occur close to the ionization front in our model. Again, the method of Laibe et al. (2020) produces constant dust density in regions where α is constant.

The right-hand panel of Fig. 1 shows a repeat of the test with α varying with height for particles with $St = 0.05$ at $z = 0$. In this case, all of the methods produce similar results close to $z = 0$, which are in good agreement with the analytical solution of Youdin & Lithwick (2007, away from the mid-plane the analytical solution is no longer valid). Again, the Ormel & Liu (2018) method shows an artefact at the transition, while in this case settling reduces the difference between our method and that of Laibe et al. (2020).

As a final confirmation of the ability of our code to deal with sharp gradients in the density, we show in Fig. 2 the density of $St = 0$ particles in an ionization front test with a width $W = 10^{-5}$ au (and $H \approx 0.89$ au). This shows excellent agreement with the background profile, as expected.

4 ANALYTICAL ESTIMATES

Here, we provide some simple estimates of the maximum size of dust grains that can be entrained in the wind. For sufficiently weak turbulence, the delivery of dust to the ionization front can be estimated by neglecting the $u_{\rm z}'$ term in equation (4): In this case, the passage of dust from the disc to the wind is simply set by the extent to which grains can couple to the advective flow of gas in the disc induced in response to mass-loss at the ionization front. The maximum size of particles delivered to the wind may be estimated as the biggest particle for which $v_z > 0$ at the ionization front, which in the terminal velocity limit may be written as

$$St_{\rm crit} = \frac{u_{\rm z}(z_{\rm IF})}{\Omega z}\left(1 + \frac{z_{\rm IF}^2}{R^2}\right)^{3/2}, \tag{13}$$

as suggested by Hutchison & Clarke (2021). Note that this refers to the Stokes number measured just below the ionization front. Since $u_z \ll c_{\rm s}$ in the disc, $St_{\rm crit}$ can be approximated as

$$St_{\rm crit} \approx \frac{\mathcal{M}_{\rm w}}{1 + \mathcal{M}_{\rm w}^2}\frac{c_{\rm s,disc}}{c_{\rm s,wind}}\frac{H}{z_{\rm IF}} = 0.4\frac{c_{\rm s,disc}}{c_{\rm s,wind}}\frac{H}{z_{\rm IF}}, \tag{14}$$

where we have used the Rankine–Hugoniot relations to relate the velocity in the disc to the Mach number at the base of the wind, $\mathcal{M}_{\rm w} = 0.5$. For typical values of $c_{\rm s,disc}$ and $c_{\rm s,wind}$, we find $St_{\rm crit} \approx 0.01$.

For comparison, the maximum particle size that, once in the wind, can escape from the disc is approximately given by the particle size for which the terminal velocity is zero at the base of the wind, i.e. down-wind of the ionization front.[4] Following, Hutchison & Clarke (2021), we refer to this as $St_{\rm max}$, which is given by

$$St_{\rm max} = (1 + \mathcal{M}_{\rm w}^2)\frac{c_{\rm s,wind}}{c_{\rm s,disc}}St_{\rm crit} \approx \mathcal{M}_{\rm w}\frac{H}{z_{\rm IF}} = 0.5\frac{H}{z_{\rm IF}}. \tag{15}$$

We emphasize that although $St_{\rm crit}$ and $St_{\rm max}$ relate to situations of force balance applied on either side of the ionization front, they relate to stopping times that are evaluated at the same location (i.e. just below the ionization front) and their ratio therefore directly relates

[4]Note that the condition that the terminal velocity is zero is equivalent to requiring a situation of zero net acceleration on a stationary particle as argued by Takeuchi, Clarke & Lin (2005) and, with some order unity corrections for the flow geometry, also by Hutchison & Clarke (2021).

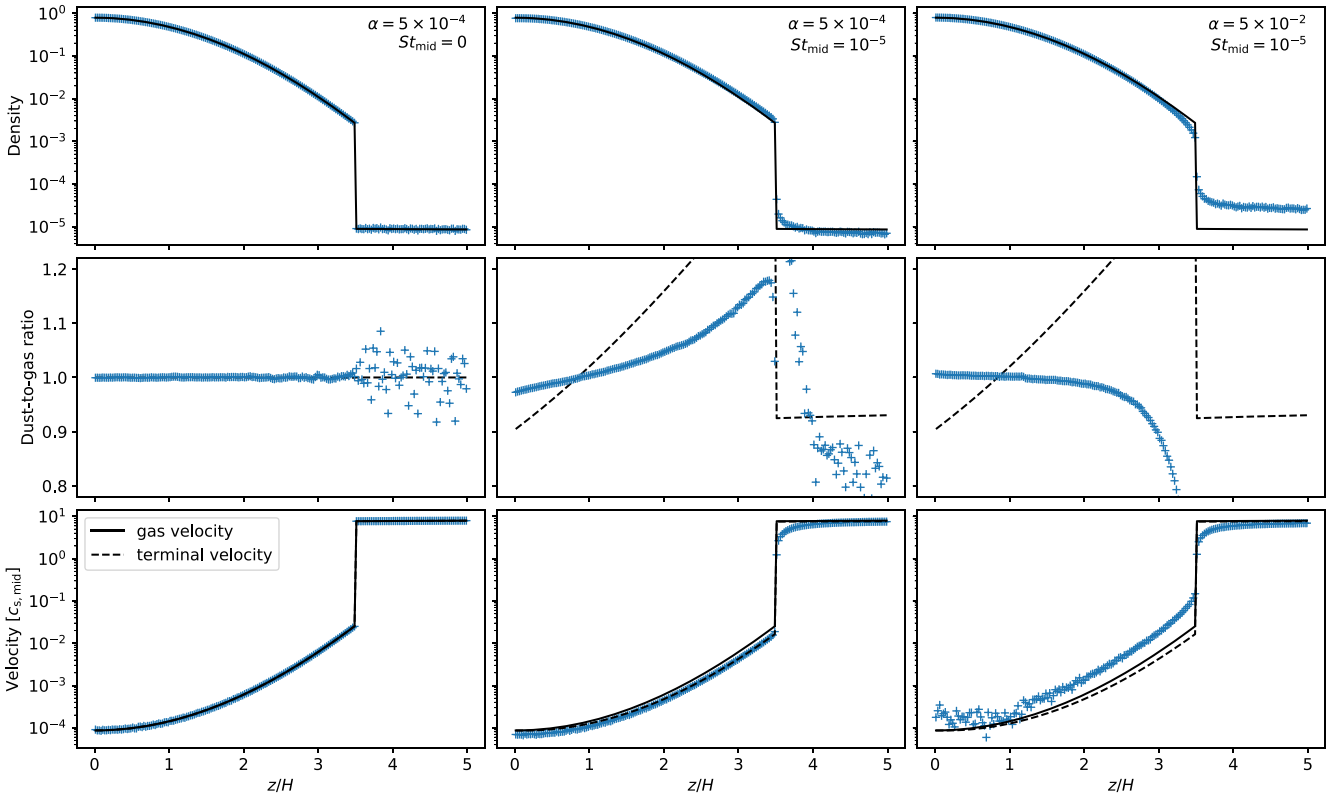

Figure 2. Vertical profiles of the density, dust-to-gas ratio, and mean velocity as a function of height for three representative simulations (columns). In each panel, the black solid lines show the gas properties from the disc model. The black dashed lines show the results expected for a purely advective solution in the terminal velocity limit.

to the ratio of dust sizes that achieve this condition on each side of the front. Comparison of equations (14) and (15) immediately shows that in the case of dust that is advected through an ionization front, the grains that are just able to reach the ionization front are a factor of $\sim \frac{c_{\rm s,disc}}{c_{\rm s,wind}}$ in size below the maximum size that can be entrained in the ionized wind. Thus, *delivery* of grains to the ionization front is the limiting step in removing dust from the disc rather than the subsequent ability of the ionized wind to carry it away (Hutchison & Clarke 2021).

When turbulence is strong, we expect that dust may be delivered to the ionization front diffusively instead of being delivered by advection. Neglecting the contribution from advection [i.e. setting $u(z) = 0$], the dust density is given by

$$\frac{\rho_{\rm d}}{\rho_{\rm g}} \propto \exp\left(-\frac{St(z)}{\alpha}\right) \tag{16}$$

(Dubrulle et al. 1995; Takeuchi & Lin 2002). Therefore, in a purely diffusive disc the delivery of dust to the ionization front should drop once $St(z_{\rm IF}) > \alpha$ (note that we have neglected the influence of the ionization front itself). Since advection can efficiently supply dust to the ionization front for sizes below $St_{\rm crit}$, we therefore expect the transition to the diffusive regime to occur at $\alpha \sim St_{\rm crit} \approx 0.01$.

5 NUMERICAL SIMULATIONS

5.1 Advective and diffusive dust delivery

For the results presented in this section, we set up the gas profile according to the description in Section 2.1. Dust particles are then injected continuously at $z = 0$ at a rate of 4Ω and the simulation is run for $10^5\Omega^{-1}$. For the boundary conditions, particles are removed once they cross $z = 5H$, while at $z = 0$ we use reflecting boundaries (i.e. particles that cross $z = 0$ have the sign of z, v_z, and $w_{\rm t}$ flipped).

The mass-loss time-scale of dust particles was computed by comparing the rate of particle injection to the total number of particles in the domain once the simulation has reached a steady state. Since for very low mass-loss rates (i.e. for $St > St_{\rm crit}$) steady state is not reached within $10^5\Omega^{-1}$, we instead fit a model to the total number of particles in the domain over time using least squares (via SCIPY's CURVE_FIT routine[5]). The model we use is

$$\frac{{\rm d}N}{{\rm d}t} = \dot{N}_0 - \frac{N}{\tau}, \tag{17}$$

where $\dot{N}_0 = 4\Omega$. We then compare τ (i.e. $N/\dot{N}_0$ in steady state) to the mass-loss time-scale of the gas $\Sigma/\dot{\Sigma}$ to determine the efficiency of dust entrainment in the wind:

$$\epsilon_{\rm F} = \frac{\Sigma}{\dot{\Sigma}\tau} = \frac{\Sigma}{\Sigma_{\rm d}}\frac{\dot{\Sigma}_{\rm d}}{\dot{\Sigma}}. \tag{18}$$

With this definition, the mass-loss rate of dust is simply the product of $\epsilon_{\rm F}$, the mass-loss rate of gas, and the dust-to-gas ratio. We note that this definition of the entrainment efficiency is slightly different to the definition used by Hutchison & Clarke (2021), who used $\dot{N}_0/(\rho_{\rm d}(z=0)u_z(z=0))$ (where $\rho_{\rm d}$ is normalized such that the total mass is 1). This choice is dictated by practicality: The definition used

[5]https://www.scipy.org/

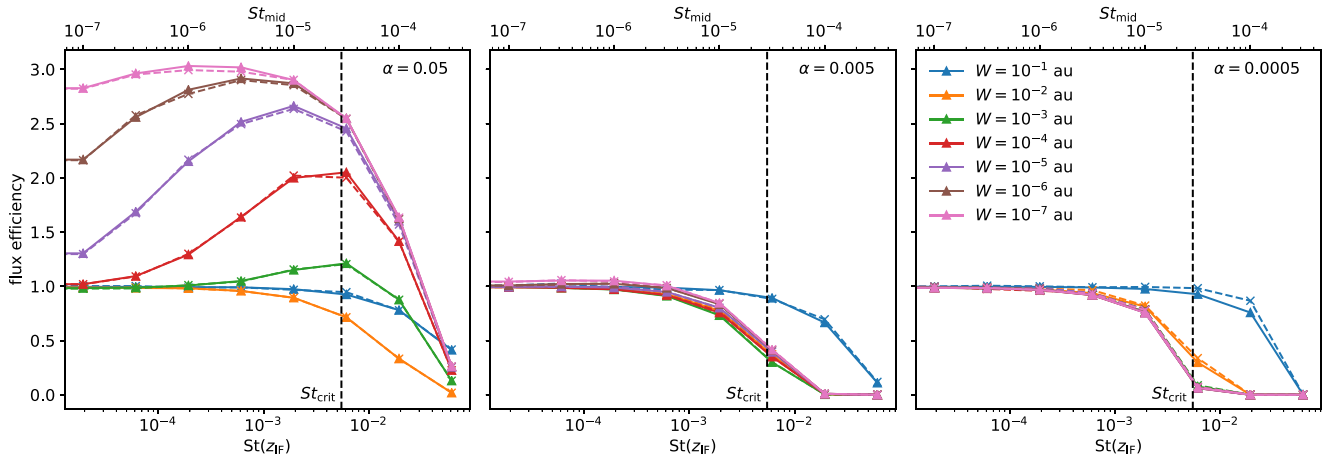

Figure 3. Flux efficiency, $\epsilon_{\rm F}$, for an ionization front model at $R = 10$ au and $z_{\rm IF} = 3.5\,H$. Each panel shows a range of ionization front widths, W, for a different strength of turbulence, α. For comparison, the flux efficiency computed using the definition in Hutchison & Clarke (2021) is shown by the dashed lines.

here is easier to determine accurately. However, the estimates only differ by a factor of $(\Sigma_{\rm g}/\Sigma_{\rm d})[\rho_{\rm d}(z=0)/\rho_{\rm g}(z=0)] \approx 1$.

For the simulations presented in this section, we choose $z_{\rm IF}$ in the approximate range of $3H$–$4H$ as a compromise between realistic mass-loss rates and computational expediency. Note the mass-loss time-scale, $\Sigma/\dot{\Sigma}$, is (approximately) given by

$$\frac{\dot{\Sigma}}{\Sigma} \approx \frac{1}{\sqrt{2\pi}} \exp\left(-\frac{z_{\rm IF}^2}{2H^2}\right) \frac{\mathcal{M}_{\rm w}}{1+\mathcal{M}_{\rm w}^2} \frac{c_{\rm s,disc}}{c_{\rm s,wind}} \Omega \tag{19}$$

$$\approx 1 \times 10^{-2} \exp\left(-\frac{z_{\rm IF}^2}{2H^2}\right) \left(\frac{R}{10\,\mathrm{au}}\right)^{-1/4} \Omega. \tag{20}$$

Therefore, $z_{\rm IF} = 4H$ corresponds to a reasonable mass-loss time-scale of 10^6 yr at $R = 10$ au.

The efficiency of dust entrainment for models with $R = 10$ au and $z_{\rm IF} = 3.5\,H$ is shown in Fig. 3 for $\alpha = (5 \times 10^{-4})$–$(5 \times 10^{-2})$ and a range of ionization front widths, W.

For small α, we find a flux efficiency $\epsilon_{\rm F} \approx 1$ for small St, transitioning to $\epsilon_{\rm F} \approx 0$ at $St \approx St_{\rm crit}$ for all but the largest of ionization front widths. This is the expected result for advection-dominated delivery of dust to the wind. Comparing the $\alpha = 5 \times 10^{-4}$ results to those $\alpha = 5 \times 10^{-3}$ shows that increasing α mildly increases $\epsilon_{\rm F}$ for St close to $St_{\rm crit}$, but in both cases $St_{\rm crit}$ remains a good estimator of the maximum dust size that can be entrained.

For $\alpha = 0.05$, the delivery of dust to the ionization front is now diffusion dominated according to our estimate in Section 4 (since $\alpha > St_{\rm crit}$), resulting in different behaviour. For $St \lesssim St_{\rm crit}$, the mass-loss rate of dust is now *higher* than that of the gas and also dependent on the width of the ionization front. We also find that for sufficiently narrow ionization fronts the dust flux eventually converges. Convergence occurs at progressively smaller ionization front widths as the Stokes number decreases. This convergence can be explained by considering the stopping distance at the two different sides of the ionization front:

$$l_{\rm disc} \approx \frac{\mathcal{M}_{\rm w}}{1+\mathcal{M}_{\rm w}^2} \frac{c_{\rm s,disc}}{c_{\rm s,wind}} St\,H = 0.4 \frac{c_{\rm s,disc}}{c_{\rm s,wind}} St\,H, \tag{21}$$

$$l_{\rm wind} \approx l_{\rm disc}(1+\mathcal{M}_{\rm w}^2) \frac{c_{\rm s,wind}}{c_{\rm s,disc}} = 0.5\,St\,H, \tag{22}$$

where in both cases the Stokes number is measured in the disc immediately before the ionization front. As the width of the ionization front is successively decreased, particles with a given Stokes number will first decouple on the down-wind side of the ionization front. Finally, once $W \ll l_{\rm disc} \approx 0.03StH$, the particles will cross the ionization front before being able to react, and thus the width of the ionization can no longer affect the flux. Fig. 3 confirms this, with convergence by $W \approx 0.1 l_{\rm disc}$.

The dependence of the flux on α can be understood by looking at the dust-to-gas ratio profiles, shown for two examples in Fig. 2. At $\alpha = 5 \times 10^{-4}$ and $St_{\rm mid} = 10^{-5}$, the dust-to-gas ratio increases with z between the mid-plane and the ionization front. This follows from mass conservation and the fact that dust velocity is lower than the gas velocity since the gravitational acceleration is not nearly balanced by pressure, as in the case of the gas, and finite $t_{\rm stop}$ prevents the dust from keeping up with the gas flow. However, already for this low α the dust-to-gas ratio gradient is lower than that predicted by the purely advective regime. This is the result of turbulent diffusion and acts to reduce the mass flux (as can be seen from Fig. 3 and also the dust-to-gas ratio being below 1 at $z = 5H$).

Increasing α, one would expect the dust-to-gas ratio to be driven towards a constant value even more strongly. However, in the simulation with $\alpha = 0.05$, we see a negative gradient in dust-to-gas ratio, evidence that diffusion is now driving an outward flux of dust (which is further supported by the average dust velocity in Fig. 2 being larger than the mean gas velocity). This gradient is particularly strong close to the ionization front. Our proposed explanation for this is that the diffusive supply of dust to the ionization front from the disc is not matched by a return flux from the wind since the low-density down-wind of the front means that such particles are not effectively coupled to turbulent motions driving them back through the front. Conversely, for particles small enough that they remain coupled to the gas through the ionization front, the diffusive flux is cancelled by the $w_{\rm hs}$ correction term resulting in $\epsilon_{\rm F} \approx 1$.

Even in the diffusive regime, the mass-loss rate of dust becomes negligible once the Stokes number exceeds $St_{\rm crit}$ by more than a factor of $\sim$10. For grains of this size, $St > St_{\rm max}$, and the drag force on particles that pass through the ionization front is no longer sufficient to overcome gravity in the wind. Therefore, even if dust can be supplied to the wind, ultimately it cannot escape the disc.

The results are not sensitive to the underlying parameters of the disc. This is demonstrated in Appendix A and Fig. 4, where we compare the Stokes number at which $\epsilon_{\rm F}$ drops to 0.5 to the values of $St_{\rm crit}$ and $St_{\rm max}$. We do this varying $z_{\rm IF}$ at $R = 10$ au (left-hand panel)

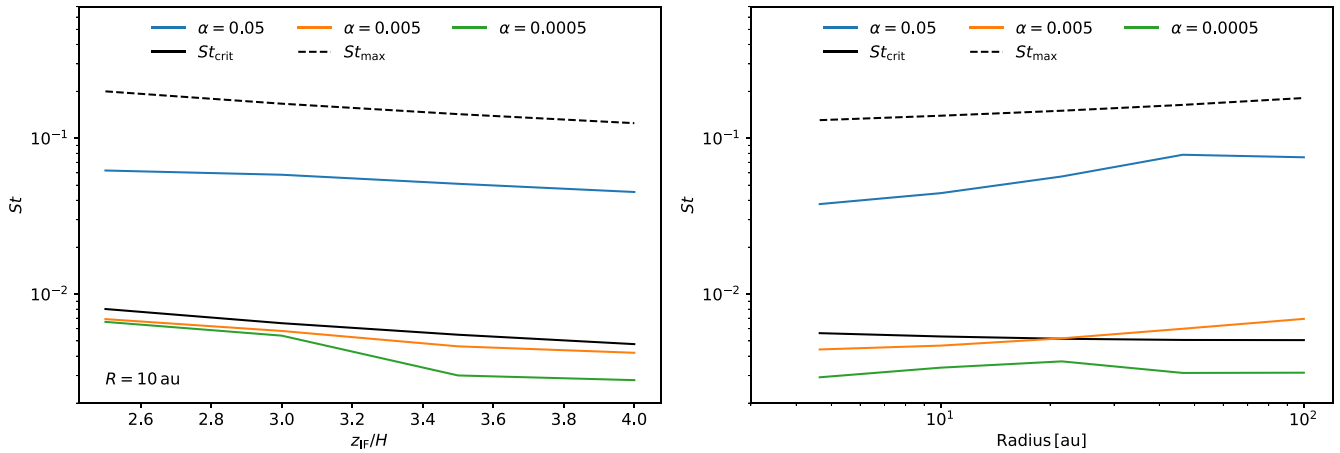

Figure 4. Comparison of the maximum size of dust grains delivered in the wind (defined as the size at which the efficiency drops below 0.5) to analytical estimates of the maximum size of grain delivered to the wind base ($St_{\rm crit}$) and carried away by the wind ($St_{\rm max}$). Left: effect of the ionization front location at $R = 10$ au. Right: variation with radius for a model with the ionization front height computed using an EUV model with an ionizing flux of $\Phi = 10^{42}\,{\rm s}^{-1}$. In each case, the Stokes number shown is the Stokes number in the disc as measured at the ionization front.

and also for a model where $z_{\rm IF}$ is computed according to equation (23) for $\Phi = 10^{42}\,{\rm s}^{-1}$. The EUV model follows Hutchison & Clarke (2021), who assume that the density at the wind base is controlled by recombination:

$$\rho_{\rm ion} = 0.2 m_{\rm H} \left(\frac{3\Phi}{4\pi\alpha_2 R^3}\right)^{1/2}, \tag{23}$$

where the velocity at the wind base is $0.5 c_{\rm s,wind}$ as before. Here, $m_{\rm H}$ is the mass of a hydrogen atom, $\alpha_2 = 2.6 \times 10^{-13}\,{\rm cm}^3\,{\rm s}^{-1}$ is the Case B recombination coefficient, and Φ is the stellar EUV luminosity.

In Fig. 4, we see that the maximum size entrained is close to $St_{\rm crit}$ for $\alpha < St_{\rm crit}$ independent of the height of the ionization front or the location in the disc. Furthermore, although the size increases above $St_{\rm crit}$ for $\alpha > St_{\rm crit}$, it always remains smaller than $St_{\rm max}$.

5.2 Typical grain sizes entrained

Now that we have ascertained that the maximum size of dust grains delivered to the wind is determined by $St_{\rm crit}$ in the advective regime while $St_{\rm max}$ limits the size of grains removed in the diffusive regime, we consider what these Stokes numbers mean in terms of grain size. From the definition of these limits (i.e. zero acceleration of a stationary grain just below and just above the ionization front, respectively), we can write

$$s_{\rm crit} = \sqrt{\frac{8}{\pi}} \frac{\dot{\Sigma}}{\rho_{\rm grain}\Omega} \frac{H_{\rm IF}}{z_{\rm IF}} \left(1 + \frac{z_{\rm IF}^2}{R^2}\right)^{3/2} \tag{24}$$

$$\approx 0.63 \left(\frac{\dot{\Sigma}}{10^{-12}\,{\rm g\,cm^{-2}\,s^{-1}}}\right) \left(\frac{R}{10\,{\rm au}}\right)^{3/2} \times \left(\frac{z_{\rm IF}}{4H_{\rm IF}}\right)^{-1} \left(\frac{M_*}{1\,{\rm M}_\odot}\right)^{-1/2} \left(\frac{\rho_{\rm grain}}{1\,{\rm g\,cm^{-3}}}\right)^{-1} \mu{\rm m}. \tag{25}$$

This shows that maximum size of dust particle that can be entrained is insensitive to the disc mass, which only enters through the dependence of $z_{\rm IF}$ on disc mass, which is weak. Note that this equation is valid even if the disc is not vertically isothermal (as assumed in this paper) as long as $H_{\rm IF}$ is determined from $c_{\rm s,disc}$ measured at the ionization front. Similarly, the definition for $s_{\rm max}$ follows by replacing $c_{\rm s,disc}$ with $c_{\rm s,wind}$ (in the definition for $H_{\rm IF}$).

We show $s_{\rm crit}$ for representative values of $\dot{\Sigma}$ and R in Fig. 5, over which we plot the mass-loss profiles from representative EUV (Hollenbach et al. 1994)- and X-ray (Picogna et al. 2019)-driven wind models assuming $z_{\rm IF} = 4{\rm H}_{\rm IF}$. Typical grain sizes vary between 0.01 and 1 μm.

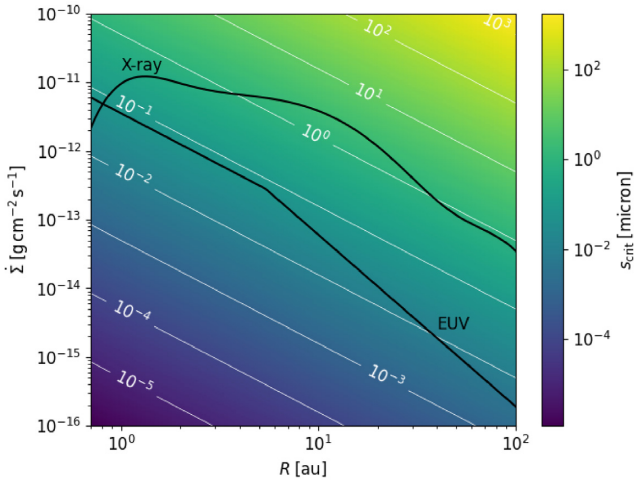

Figure 5. Maximum size of dust particles that can be delivered to a photoevaporative wind for a given mass-loss rate per unit area and radius (colour map and white contours). The black lines show the mass-loss profiles for the EUV-driven wind model with $\Phi = 10^{42}\,{\rm s}^{-1}$ (Hollenbach et al. 1994) and X-ray-driven wind with $L_{\rm X} = 2 \times 10^{30}\,{\rm erg\,s}^{-1}$ (Picogna et al. 2019), for which the integrated mass-loss rates are 7.4×10^{-10} and $2.7 \times 10^{-8}\,{\rm M}_\odot\,{\rm yr}^{-1}$, respectively. Note that $s_{\rm crit}$ is given here for the case $\rho_{\rm grain} = 1\,{\rm g\,cm^{-3}}$ and an ionization front height of $z_{\rm IF} = 4H$ and scales with $H/z_{\rm IF}\rho_{\rm grain}$ (equation 25).

These values of $s_{\rm crit}$ can be estimated analytically from the mass-loss rates, i.e. in the case of an EUV-driven wind with density profile given by (23) (as is appropriate to disc radii interior to $R_{\rm g} = GM_*/c_{\rm s,wind}^2 \approx 5$ au)

$$s_{\rm crit,\,EUV} = 0.2 \left(\frac{6\Phi}{GM_*\alpha_2\pi^2}\right)^{1/2} \frac{m_{\rm H} v_{\rm wind}}{\rho_{\rm grain}} \frac{H_{\rm IF}}{z_{\rm IF}} \tag{26}$$

$$\approx 0.022 \left(\frac{\Phi}{10^{41}{\rm s}^{-1}}\right)^{1/2} \left(\frac{M_*}{1\,{\rm M}_\odot}\right)^{-1/2} \left(\frac{z_{\rm IF}}{4H_{\rm IF}}\right)^{-1} \mu{\rm m}. \tag{27}$$

Note that in the original model of Hollenbach et al. (1994), the density at the ionization front falls off more steeply with radius beyond R_g, scaling as $R^{-2.5}$, outside the gravitational radius: This effect has been included in the estimate for $\dot{\Sigma}(R)$ in the EUV case shown in Fig. 5.

A simple estimate for $s_{\rm crit}$ in X-ray-driven winds may be estimated from $\dot{\Sigma} \sim 2 \times 10^{-12} (R/10\,{\rm au})^{-3/2}\,{\rm g\,cm^{-2}\,s^{-1}}$ for an X-ray luminosity, $L_{\rm X} = 2 \times 10^{30}\,{\rm erg\,s^{-1}}$ (Picogna et al. 2019). The corresponding estimate for the maximum grain size entrained is then

$$s_{\rm crit,\,X\text{-}ray} \sim 1 \times \left(\frac{L_{\rm X}}{2 \times 10^{30}\,{\rm erg\,s^{-1}}} \right) \left(\frac{z_{\rm IF}}{4 H_{\rm IF}} \right)^{-1} \mu{\rm m}. \tag{28}$$

More precise numbers can be obtained by directly using the fits for $\dot{\Sigma}$ provided by Picogna et al. (2019), which were used in Fig. 5.

Finally, the distribution of dust entrained in the wind can be computed from the flux efficiency, $\epsilon_{\rm F}$ (Fig. 3). Since $\epsilon_{\rm F}$ falls off rapidly for $St > St_{\rm crit}$, the contribution from sizes much beyond $St_{\rm crit}$ can be neglected.

6 DISCUSSION

In this paper, we have demonstrated that the removal of dust from protoplanetary discs by winds is driven by advection unless turbulence in the disc is strong, i.e. $\alpha \gtrsim St_{\rm crit} \approx 0.01$ (equation 14). Note that $St_{\rm crit}$ is measured in the disc immediately below the ionization front and thus varies only weakly with system parameters (see Fig. 4), being mainly set by the difference in temperature between the disc and the ionized wind. We find that strong turbulence acts to increase the amount of dust supplied to the wind by a factor of a few in certain size ranges (see the left-hand panel of Fig. 3), rather than decreasing it, as was found by Hutchison & Clarke (2021). This difference can be attributed to the way in which diffusion was treated in the two studies. Hutchison & Clarke (2021) treated diffusion by adding a diffusive flux to the mass-conservation equation using the model of Dubrulle et al. (1995). Here, we have used a Monte Carlo model for the dust in which diffusion is treated through the direct coupling of dust to turbulent motions in the disc gas via drag forces, modelling the turbulence assuming isotropic Gaussian turbulence with a constant velocity dispersion. The explanation for this difference is that if one simply adds a diffusive flux using the Dubrulle et al. (1995) model, it implies an increase in the dust-to-gas ratio across the front which can drive a strong negative diffusive flux. The reason why this does not happen in reality is that, as particles cross the ionization front, they decouple from the gas flow and do not participate in diffusive motions. This behaviour can only be captured by a treatment that explicitly models the ability of particles with finite stopping time to decouple from the diffusive motions over a region where there is a steep gradient in background gas properties. We therefore caution against applying the Dubrulle et al. (1995) model in situations involving ionization fronts.

Although isotropic turbulence is likely a poor approximation at the ionization front, our results are unlikely to be substantially affected by this. This is obviously the case when the delivery of dust is dominated by advection, which is the case for both weak turbulence and sufficiently small particles in the regime of strong turbulence. Since large particles cross the ionization front within a stopping time, they cannot couple to the gas within the ionization front, and therefore the details of the turbulence at the ionization are not important. For intermediate grain sizes in conditions of strong turbulence, particles begin to decouple within the ionization front. The mass-loss rate of these particles is sensitive to the width of the ionization front, and therefore possibly also sensitive to details of the turbulence there. However, the dependence of the flux on the properties of the ionization front is weak, and the phenomenological behaviour is unlikely to be affected.

Our results suggest that vertical advective transport in discs could play an important role in determining the vertical height of discs measured in scattered light. Recent non-ideal MHD simulations suggest that discs may have weak turbulence ($\alpha \lesssim 10^{-4}$), with observational studies providing supporting evidence (see e.g. Mulders & Dominik 2012; Flaherty et al. 2015; Simon et al. 2018; Flaherty et al. 2020). Under such conditions, our models show that advective transport due to the wind should dominate the lofting of small grains – this could be tested by comparing resolved observations of disc thickness in the scattered light to the thickness derived for millimetre grains (e.g. Pinte et al. 2016; Avenhaus et al. 2018; Villenave et al. 2020). If turbulence is stratified, i.e. α increases with height, then turbulence might still play an important role. However, Riols & Lesur (2018) found that the vertical variation of α could not explain the lofting of grains seen in their MHD simulations unless advective transport was also included. We suggest that this is likely to be a general feature of discs undergoing mass-loss due to winds, independent of the winds' origin.

In our calculations, we have neglected the influence of radiation pressure on the dust grains. Since the optical photosphere is at lower altitudes than the EUV (or X-ray) photosphere, Owen & Kollmeier (2019) argued that radiation pressure could remove grains efficiently. We now show that when including advective transport, radiation pressure does not greatly change the picture. Neglecting turbulence, but including radiation pressure, the vertical and radial velocities of dust grains are, respectively, given by

$$v_z = v_g - (1-\beta)\Omega z St, \tag{29}$$

$$v_R = \beta \Omega R St, \tag{30}$$

where β is the ratio of the radiation pressure force to the gravitational force. Here, we have assumed that β is large enough that the radiation pressure term dominates over all other components (such as the radial gas pressure gradient) in the equation for v_R from Owen & Kollmeier (2019). Rewriting the gas velocity in terms of $St_{\rm crit}$, we find

$$\frac{v_z}{v_R} = \frac{z}{R}\left[1 + \frac{1}{\beta}\left(\frac{St_{\rm crit}}{St} - 1\right)\right]. \tag{31}$$

If the height of the ionization front scales as $z_{\rm IF} \sim R^{1+\delta}$, then particles with $St \lesssim St_{\rm crit}/(1+\beta\delta)$ will be delivered to the wind. For typical values of β, the maximum grain size delivered to the wind is not much affected. Note that although radiation pressure can increase the maximum size of particles that can be entrained when $\delta < 0$, this is not the case for our EUV model with $\Sigma \propto 1/R$. Another factor that could reduce the size entrained would be if there was a steep dependence of $s_{\rm crit}$ with radius, such that radiation pressure drives the grains to larger radii where they can no longer be entrained. However, given that the dependence of $s_{\rm crit}$ is not particularly strong (Fig. 5), this will also not dramatically affect the maximum size of grains delivered to the winds.

7 CONCLUSIONS

We have investigated the entrainment of dust grains in photoevaporative winds using a novel Monte Carlo dust dynamics model that correctly models dust transport across the ionization front separating the disc and ionized wind. This treatment avoids spurious effects previously found when solving the advection–diffusion equation in the limit that the width of the ionization front is less than the dust stopping distance. Our calculations yield dust transport efficiencies

that converge in the limit of narrow ionization fronts as expected. We highlight that special care needs to be taken in the choice of Monte Carlo dust modelling algorithm in the demanding case of a steep density feature such as an ionization front and that algorithms in the literature produce numerical artefacts under these conditions.

Our simulations show that the delivery of dust to the wind base is dominated by the advection of small dust grains by the vertical gas flow that appears as a consequence of the photoevaporative mass-loss. This is contrary to the usual assumption that turbulent diffusion is responsible for lofting grains to the ionization front, which we show only occurs if disc turbulence is strong (i.e. for values of the Shakura & Sunyaev 1973 α-parameter $\gtrsim 0.01$).

Our results confirm the hypothesis of Hutchison & Clarke (2021) that the maximum size of dust grains entering the wind is set by the condition of zero force on a stationary dust grain immediately below the ionization front (a limit that we denote as $s_{\rm crit}$). This is *not* the same as the commonly assumed limit (which, following Hutchison & Clarke 2021, we designate $s_{\rm max}$) that corresponds to the condition of zero force on a stationary dust grain immediately above the ionization front. The drag force scales as the product of the gas flux and the local sound speed: Since the flux is conserved across the front, this means that the ratio of $s_{\rm crit}$ to $s_{\rm max}$ is given by the ratio of local sound speeds, and is thus typically around $\sim$0.1 in the case of ionized winds from protostellar discs. Equation (25) allows the value of $s_{\rm crit}$ to be estimated for any wind where the local mass flux and height of the base of the heated region are known; Fig. 5 illustrates the typical values that apply in the case of mass-loss profiles for canonical EUV- and X-ray-driven winds. These values are lower by around a factor of 10, for equivalent parameters, than those previously proposed (Takeuchi et al. 2005; Owen et al. 2011a; Franz et al. 2020), a result that we ascribe to the aforementioned difference between $s_{\rm crit}$ and $s_{\rm max}$.

ACKNOWLEDGEMENTS

We thank Mark Hutchison for many interesting discussions on this topic and James Owen for encouraging us to look into radiation pressure. RAB and CJC acknowledge support from the STFC consolidated grant ST/S000623/1. This project has received funding from the European Research Council (ERC) under the European Union's Horizon 2020 research and innovation programmes PEVAP (grant agreement number 853022) and DUSTBUSTERS (grant agreement number 823823). This work was performed using the Cambridge Service for Data Driven Discovery (CSD3), part of which is operated by the University of Cambridge Research Computing on behalf of the STFC DiRAC HPC Facility (www.dirac.ac.uk). The DiRAC component of CSD3 was funded by BEIS capital funding via STFC capital grants ST/P002307/1 and ST/R002452/1 and STFC operations grant ST/R00689X/1. DiRAC is part of the National e-Infrastructure.

DATA AVAILABILITY

The simulation code used in this project is available on github at https://github.com/rbooth200/MC_dust and the simulation results will be shared upon reasonable request.

REFERENCES

Avenhaus H. et al., 2018, ApJ, 863, 44
Bai X.-N., 2017, ApJ, 845, 75
Béthune W., Lesur G., Ferreira J., 2017, A&A, 600, A75
Ciesla F. J., 2010, ApJ, 723, 514
Clarke C. J., Alexander R. D., 2016, MNRAS, 460, 3044
Clarke C. J., Gendrin A., Sotomayor M., 2001, MNRAS, 328, 485
Dubrulle B., Morfill G., Sterzik M., 1995, Icarus, 114, 237
Ercolano B., Koepferl C., Owen J., Robitaille T., 2015, MNRAS, 452, 3689
Ercolano B., Jennings J., Rosotti G., Birnstiel T., 2017, MNRAS, 472, 4117
Flaherty K. M., Hughes A. M., Rosenfeld K. A., Andrews S. M., Chiang E., Simon J. B., Kerzner S., Wilner D. J., 2015, ApJ, 813, 99
Flaherty K. et al., 2020, ApJ, 895, 109
Franz R., Picogna G., Ercolano B., Birnstiel T., 2020, A&A, 635, A53
Fritsch F. N., Carlson R. E., 1980, SIAM J. Numer. Anal., 17, 238
Gorti U., Liseau R., Sándor Z., Clarke C., 2016, Space Sci. Rev., 205, 125
Hollenbach D., Johnstone D., Lizano S., Shu F., 1994, ApJ, 428, 654
Hutchison M. A., Clarke C. J., 2021, MNRAS, 501, 1127
Hutchison M. A., Laibe G., Maddison S. T., 2016, MNRAS, 463, 2725
Laibe G., Bréhier C.-E., Lombart M., 2020, MNRAS, 494, 5134
Miotello A., Robberto M., Potenza M. A. C., Ricci L., 2012, ApJ, 757, 78
Mulders G. D., Dominik C., 2012, A&A, 539, A9
Ormel C. W., Liu B., 2018, A&A, 615, A178
Owen J. E., Kollmeier J. A., 2019, MNRAS, 487, 3702
Owen J. E., Ercolano B., Clarke C. J., 2011a, MNRAS, 411, 1104
Owen J. E., Ercolano B., Clarke C. J., 2011b, MNRAS, 412, 13
Picogna G., Ercolano B., Owen J. E., Weber M. L., 2019, MNRAS, 487, 691
Pinte C., Dent W. R. F., Ménard F., Hales A., Hill T., Cortes P., de Gregorio-Monsalvo I., 2016, ApJ, 816, 25
Press W. H., Teukolsky S. A., Vetterling W. T., Flannery B. P., 2007, Numerical Recipes: The Art of Scientific Computing, 3rd edn. Cambridge Univ. Press, Cambridge
Riols A., Lesur G., 2018, A&A, 617, A117
Salmeron R., Königl A., Wardle M., 2007, MNRAS, 375, 177
Sellek A. D., Booth R. A., Clarke C. J., 2020, MNRAS, 492, 1279
Shakura N. I., Sunyaev R. A., 1973, A&A, 500, 33
Simon J. B., Bai X.-N., Flaherty K. M., Hughes A. M., 2018, ApJ, 865, 10
Suzuki T. K., Inutsuka S.-i., 2009, ApJ, 691, L49
Takeuchi T., Lin D. N. C., 2002, ApJ, 581, 1344
Takeuchi T., Clarke C. J., Lin D. N. C., 2005, ApJ, 627, 286
Thomson D. J., 1984, Q. J. R. Meteorol. Soc., 110, 1107
Thomson D. J., 1987, J. Fluid Mech., 180, 529
Throop H. B., Bally J., 2005, ApJ, 623, L149
Villenave M. et al., 2020, A&A, 642, A164
Wilson J. D., Legg B. J., Thomson D. J., 1983, Bound.-Layer Meteorol., 27, 163
Youdin A. N., Lithwick Y., 2007, Icarus, 192, 588

APPENDIX A: EXTRA FLUX-EFFICIENCY PLOTS

In Figs A1 and A2, we show the flux efficiency, $\epsilon_{\rm F}$, for models with ionization front heights, $z_{\rm IF}$ of $3H$ and $4H$, respectively. The results are nearly identical to case with $z_{\rm IF} = 3.5H$ presented in Section 5.

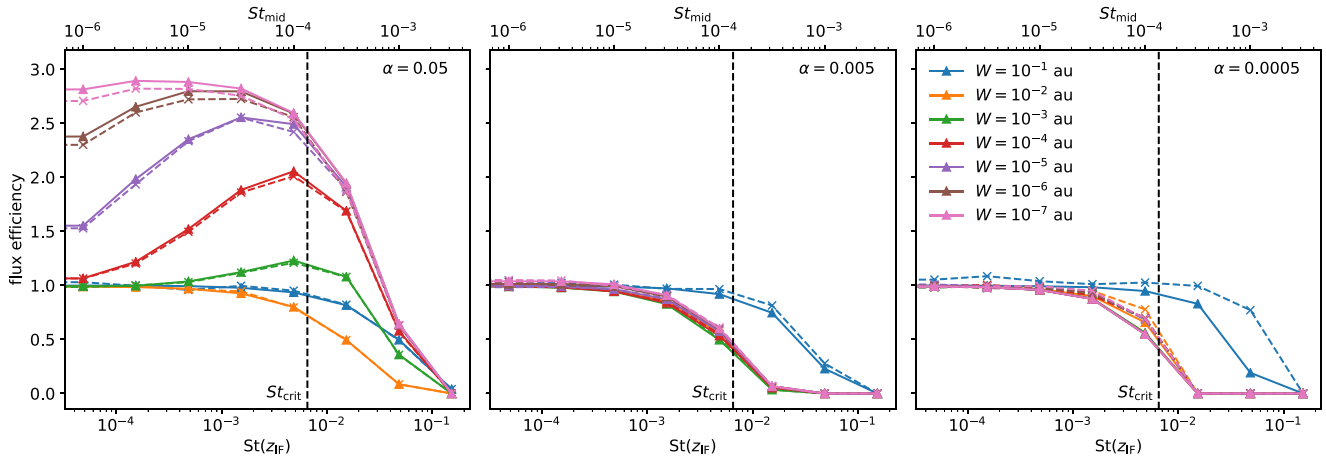

Figure A1. Same as Fig. 3 but for a model with an ionization height $z_{IF} = 3H$.

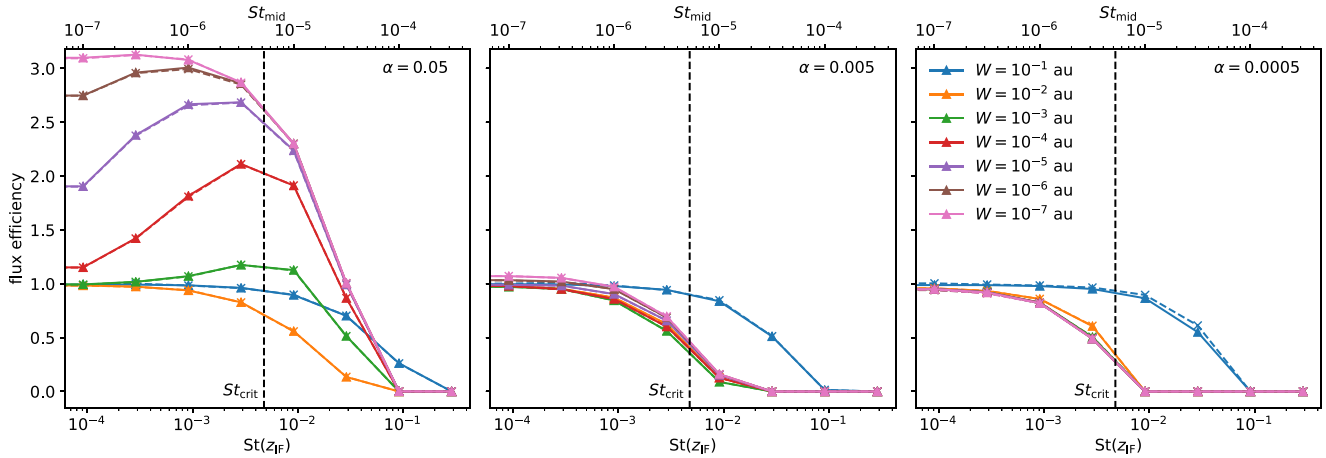

Figure A2. Same as Fig. 3 but for a model with an ionization height $z_{IF} = 4H$.

This paper has been typeset from a TEX/LATEX file prepared by the author.